Influence of structural damages on first passage time maps

K. Theunissen [1,2]**, E. Verstraelen** [3]**, J.-C. Golinval** [4]**, V. Denoël** [1]
[1] University of Liège, Department of ArGEnCo,
Allée de la Découverte 9, 4000, Liège, Belgium

[2] F.R.S.-FNRS, National Fund for Scientific Research,
Rue d'Egmont 5, B - 1000, Bruxelles, Belgium

[3] V2i S.A.,
Avenue du Pré Aily 25, 4031, Angleur, Belgium

[4] University of Liège, Department of Aérospatiale & Mécanique,
Allée de la Découverte 9, 4000, Liège, Belgium

Abstract
Current damage detection methods usually rely on changes in modal properties. Another approach, based on the mathematical concept of First Passage Time (FPT), is considered here. The FPT is defined as the time required for a signal to reach a target level X_f, starting from a level X_0. This information can be computed, through a suited algorithm for various combinations of X_0 and X_f at once, as maps of any statistical moment of FPT and even as Probability Density Functions (PDFs) of FPT. In this paper, by comparing a reference case and three damaged cases of a simple structure, it has been observed and validated that the PDFs of FPT are significantly different while the natural frequencies show no or slight difference. Therefore, the FPT can capture slight structural behavioral changes and then becomes a promising useful tool for early damage detection.

1 Introduction

The mathematical concept of First Passage Time (FPT) applied to signal processing is defined as the time required for a signal to reach a target level X_f, starting from a level X_0. Computing the FPT for varying values of X_0 and X_f provides an FPT map. For systems subject to stochastic input or governed by random parameters, the FPT is a random variable. The map therefore represents any statistical information about the FPT such as the cumulants [1, 2] or even the whole probability distribution. The map of the PDF of the FPT is a collection of Probability Density Functions (PDF) of the FPT for various combinations of X_0 and X_f. These maps provide insightful information about the studied system, as recently illustrated with tower cranes subjected to turbulent wind [3], generic systems described by the Mathieu equation [1], or a pre-stressed steel strip [4, 5].

A novel algorithm has been developed to efficiently compute such FPT maps [6]. This algorithm only goes through the whole signal once and realizes online statistical evaluation of the FPT. These two aspects make it faster and require less storage than in its previous versions [3, 5]. The new algorithm is also capable of computing the PDF of the FPT, which was not available before, and provides, therefore, richer information. Moreover, the algorithm has been validated numerically using well-known stochastic processes such as the Ornstein-Ulhenbeck process and the Geometric Brownian Motion. The advantage of these theoretical stochastic processes is that analytic solutions of their FPT cumulants and their PDFs exist.

The purpose of this work is to use the FPT algorithm in order to detect slight structural modifications of a pre-stressed steel strip [4, 5]. First of all, the experimental setup is shown and explained. Then, the results are analyzed. The PSDs are drawn in order to get a frequency which is used by current damage detection

Table 1: (a) Geometrical properties of the structure and (b) Material properties of the carbon steel structure

(a)

Parameter	Value	Units
Length	501	mm
Width	25	mm
Thickness	0.4	mm
Hanging mass	1.816	kg

(b)

Parameter	Value	Units
Density	7767	kg/m³
Young's modulus	206	GPa
Poisson's ratio	0.33	[-]

methods by comparing a reference state and a damaged state. Next, the FPT algorithm computes the average FPT maps and the STD of FPT maps. Finally, the PDFs of FPT are obtained and superimposed to detect discrepancies between the reference case and the damaged cases.

2 Materials and methods

All experimental tests are carried out at the *LTAS-Vibrations et Identification des structures* (LTAS-VIS) laboratory unit of the Department of Aerospace and Mechanical Engineering at the University of Liège. The experimental specimen is the same pre-stressed steel strip as in [4]. The geometrical and material properties of the structure are given in Tables 1(a) and 1(b). Two electrodynamic vibration shakers are mounted and shown in Figure 1(a). Only the horizontal shaker that causes a forced excitation will be used. Moreover, one impedance head is placed on the shaker to measure the acceleration and the force at these two locations. The strip is clamped on both sides and prestressed by a hanging mass at its bottom side just above the vertical shaker. A Polytec MSA-400 OFV-552 laser transducer measures the velocity of the strip at point P_3, see Figure 1(b).

To modify the structural properties of the strip a small neodymium cubic magnet is used. This magnet can be seen in Figure 1(c). The side length of this magnet is 5mm and its weight is 0.95g. Its ID article is W-05-N50-G from supermagnete [7]. Three different locations for the magnet have been used in order to identify three damage levels applied on the strip. These three locations are written P_i with $i = 1, 2$ or 3 and are shown in Figure 1(b).

3 Results and discussion

The different results have been obtained by using a narrow-band signal input whose PSD is constant in $[0.9f_0; 1.1f_0]$, where $f_0 = 39.25$Hz is the frequency of the second bending mode. Before analyzing the results obtained with the FPTs, the PSDs of the normalized velocity at point P_3 are drawn in Figure 2 when the magnet is at three different locations P_i. This normalization is simply the signal divided by its STD. These PSDs are compared to the PSD of the reference state when no magnet is put on the strip. It can be seen that the PSDs when the magnet is at points P_1 and P_2 are close to the PSD of the reference state. The shape of these PSDs is nearly superimposed and no major difference can be observed easily. However, a clear distinction can be made when the magnet is at point P_3. Indeed, even the measured value of the frequency is different and is equal to 38.19Hz, which represents a difference of 2.7% compared to the reference frequency f_0 (39.25Hz). Therefore, this damaged case is chosen and it is shown next that the FPT-based detection algorithm is capable of similar default detection performances.

One major advantage of the FPT algorithm is its ability to dissociate the fast dynamical response from the low dynamical response as explained in [1, 2] where three different regimes have been identified on FPT maps for the stochastic Mathieu equation. Therefore, the envelope of the velocity is used by this algorithm. This envelope is obtained based on the Hilbert transform [8]. The Hilbert transform of a real narrow-band signal $V(t)$ is written $\hat{V}(t)$ and is the convolution between $V(t)$ and the impulse response function $h(t) = \frac{-1}{\pi t}$. The signal $\hat{V}(t)$ is also real. It can be demonstrated that $V(t)$ and $\hat{V}(t)$ are uncorrelated for a given time t.

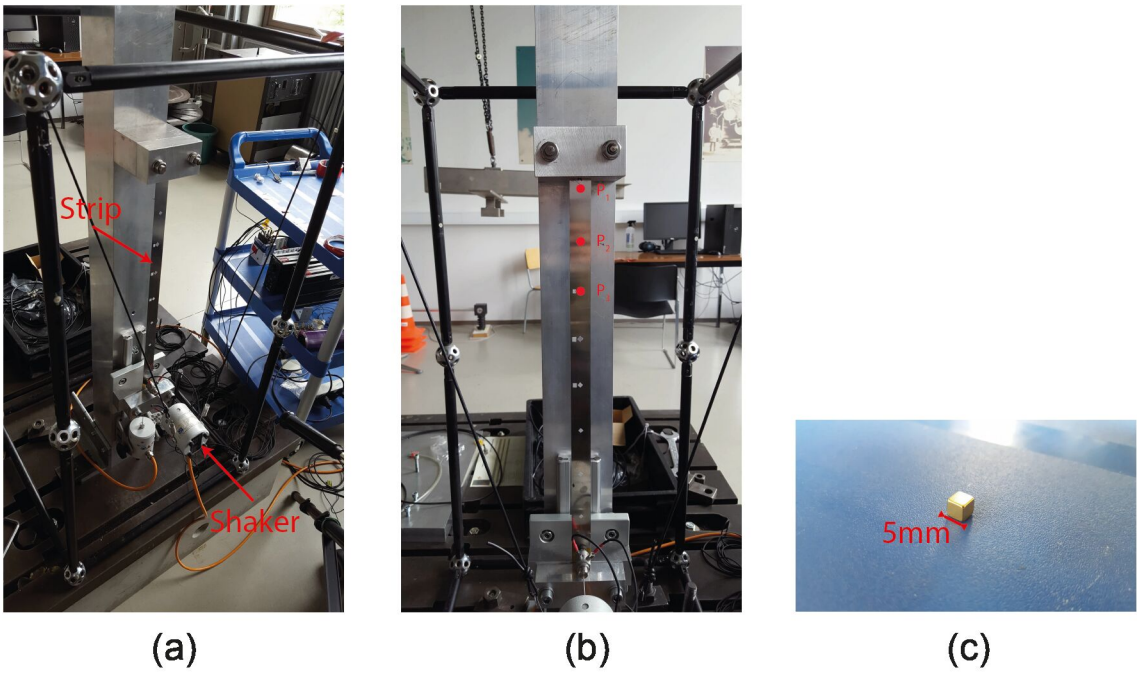

Figure 1: (a) Experimental setup side view, (b) Experimental setup front view and (c) Cubic magnet

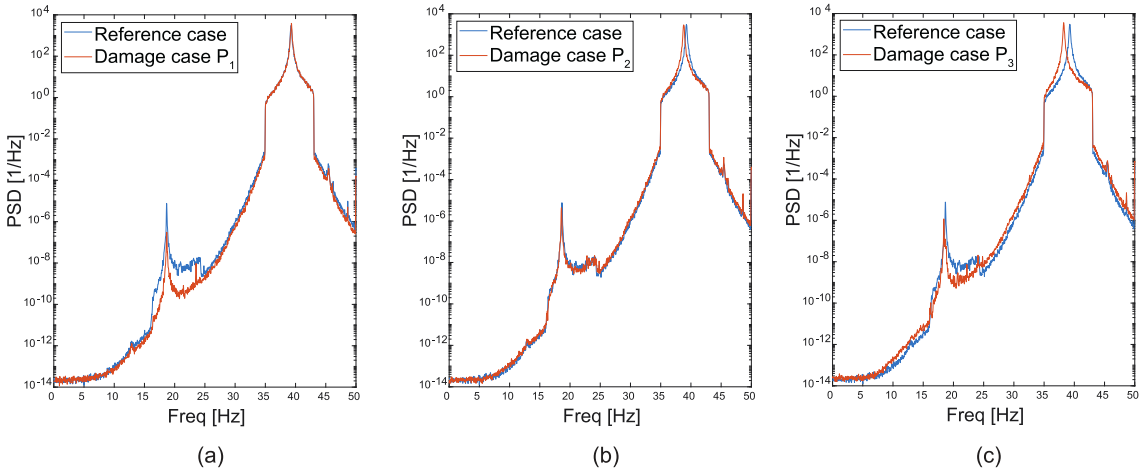

Figure 2: PSDs of the normalized velocity: Comparison between the PSD of the reference case and the PSD of the damaged case when the magnet is at (a) P_1, (b) P_2 and (c) P_3

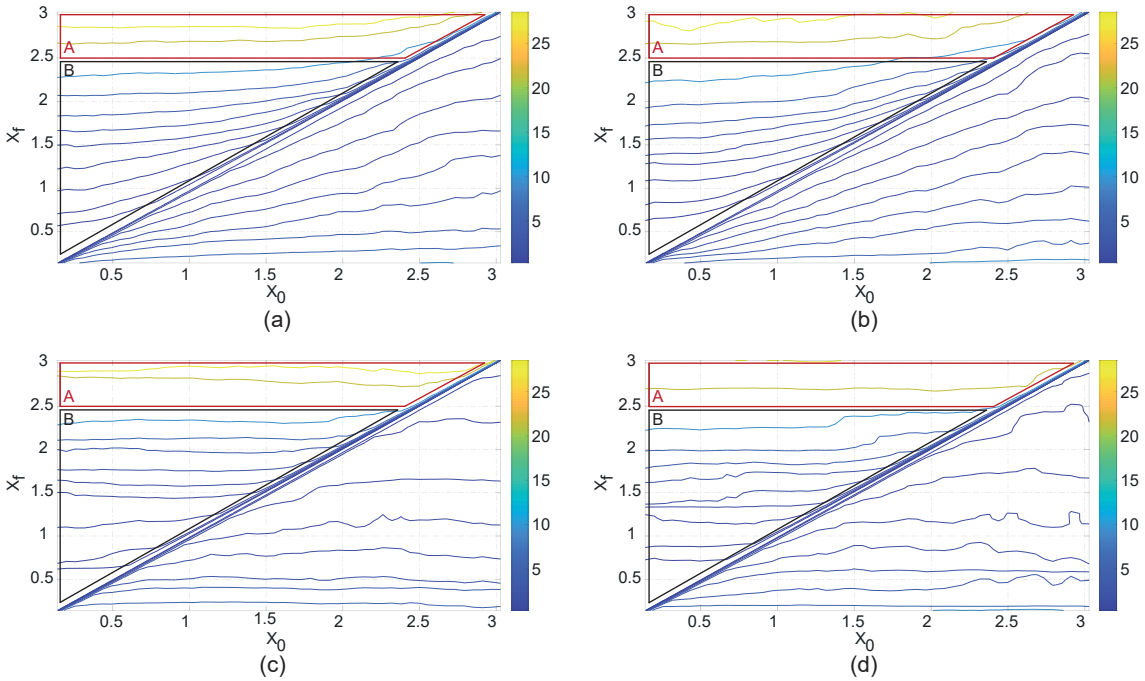

Figure 3: (a) Average FPT map of the reference case, (b) Average FPT map of the damaged case when the magnet is at point P_3, (c) STD of FPT map of the reference case and (d) STD of FPT map of the damaged case when the magnet is at point P_3

Hence, $V(t)$ and $\hat{V}(t)$ are independent random variables for a given time t. The equation of the envelope $X(t)$ defined by Cramer and Leadbetter is given by Equation (1).

$$X(t) = \left[V^2(t) + \hat{V}^2(t)\right]^{1/2} \tag{1}$$

In this paper, we compute the FPT of $X(t)$ only. The average FPT maps and the STD of FPT maps given by the algorithm are drawn in Figure 3. Figure 3(a) represents the average FPT map of the reference case and Figure 3(b) is the average FPT map when the magnet is at point P_3. Two regions are defined on these maps. Region A shows a very high average FPT with a sharp increase for a small increment of X_f while region B is wider and contains a smaller average FPT. By comparing Figure 3(a) and Figure 3(b) side by side, some differences can be observed based on the intersection locations between the contour lines and the grid. In region B, these variations are slightly visible while in region A the distinction is more obvious especially just below the top border. Indeed, due to the minor structural modification caused by the magnet at Point P_3, high values of X_f detect small modifications in the signal more easily. Hence, the average FPT is more sensitive to slight structural response changes in Region A than in Region B.

A similar discussion can be hold for Figures 3(c) and 3(d), which represent the STD of FPT in the reference case and in the damaged case when the magnet is at point P_3, respectively.

The information computed by the FPT algorithm is richer than only the frequency obtained from PSDs. Instead of focusing the analysis only on statistical moments of FPT, it is also possible to get more detailed information about FPTs by drawing their PDFs. These PDFs can be computed for each set of $\{X_0, X_f\}$. To determine the best combinations of $\{X_0, X_f\}$, the number of occurrences plays a major role in the quality of estimated PDFs. In Figure 4, the occurrences for all $\{X_0, X_f\}$ are shown for the reference case (Figure 4(a)) and for the damaged case when the magnet is at point P_3 (Figure 4(b)). In these two Figures, it can be seen that the maximum of occurrence is around $X_0 = 1$. Indeed, because each signal of velocity has first been normalized by its STD, most of the points of its envelope are located around the value 1. Based on this observation, four PDFs {I, II, III, IV} will be computed at four different locations that can be seen in Figure 4.

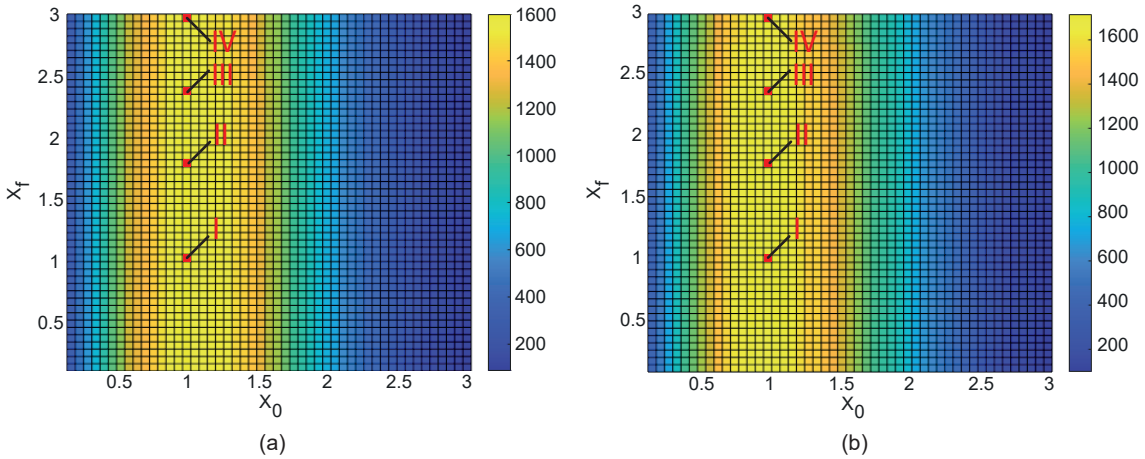

Figure 4: Occurrence of FPT map: (a) reference case and (b) damaged case when the magnet is at point P_3

In Figure 5, the PDFs of FPT at point I are shown for the reference case and the damaged case when the magnet is at point P_3. The PDFs in dotted lines are computed for one test of twenty minutes. The number of tests in each configuration is three. The two solid lines represent the PDFs by taking into account all FPTs of these three tests. Therefore, these solid lines can be seen as an average PDF for each case. These PDFs show the richness of the information computed by the FPT algorithm. Indeed, the PDFs are bimodal. The two peaks are visible thanks to the logarithmic scale of the x-axis. The order of magnitude separating these two peaks is around 1. This shape can be explained based on the behavior of the envelope. Once the level $X_0 = 0.96$ has been reached by the signal, if the envelope is growing, a short time is required to reach the level $X_f = 1.02$. However, if the envelope is dropping, the time required before reaching the level $X_f = 1.02$ is much higher, at least one order of magnitude. Indeed, if the envelope is lower than $X_0 = 0.96$ then it oscillates during a long time before finally reaching the level $X_f = 1.02$. Despite this interesting bimodal behavior, no significant difference is observed between the two distributions of FPT in the reference and damaged cases.

In Figure 6, the PDFs of FPT for points II, III, and IV are shown. In Figures 6(a) and 6(b), no clear distinction can be made between the reference case and the damaged case when the magnet is at point P_3. Indeed, as mentioned previously, these PDFs are located in Region B. Some slight differences appear in this region by comparing the average FPT maps and the STD of FPT maps in Figure 3 but no major change can be deduced from the PDF shape. However, there is an obvious discrepancy between the reference case and the damaged case in Figure 6(c) which is located just below the top border of Region A. The PDF shape in the damage configuration is much tighter which results in a higher peak. Moreover, the location of the peaks of the reference case and of the damaged case is different.

In order to validate these observations, the absolute differences of the average $\bar{m}$, the STD $\bar{\sigma}$, the skewness $\bar{\gamma_3}$ and the kurtosis $\bar{\gamma_4}$ of FPT have been used as indicators. The goal of these indicators is to detect if the difference between the statistical moments of FPT in the reference case and in the damaged case is significant or not. Each test has been repeated three times for each configuration. Therefore, there are three experimental measures of each statistical moment of FPT. The null hypothesis is the equivalence in the distribution of each statistical moment. In other words, it means that the distribution of average FPT, for example, in the reference case is identical to the distribution of means of FPT in the damaged case. Hence, it is supposed that the average and the STDs of the statistical moments of FPT in the reference case are equal to the average and the STDs of the statistical moments of FPT in the damaged case respectively. The distribution of these differences for each statistical moment is supposed Normal whose mean is equal to zero and whose STD is $\sqrt{2}\sigma$ with σ the STD of the statistical moments of FTP. Therefore, the null hypothesis is either accepted (A) if the p-values of the absolute differences of the statistical moments in the reference case and in the damaged case are greater than $\alpha = 0.05$ or rejected (R).

In Table 2, the p-values are listed. It can be observed that $\bar{\gamma_3}$ and $\bar{\gamma_4}$ reject the null hypothesis at point IV. These indicators confirm that there is a discrepancy between the PDF of the reference and the PDF of the the

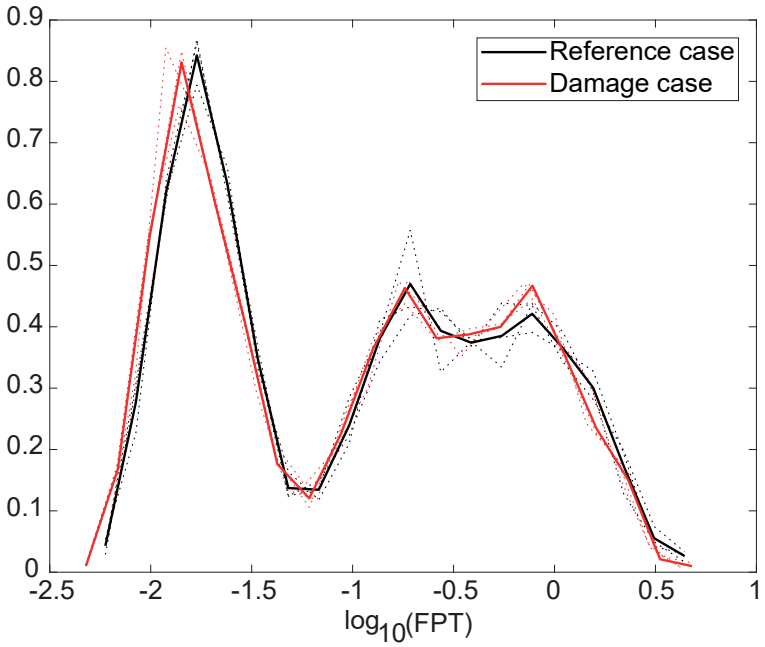

Figure 5: PDFs of FPT when $X_0 = 0.96$ and $X_f = 1.02$ (point I) for the reference case and the damaged case

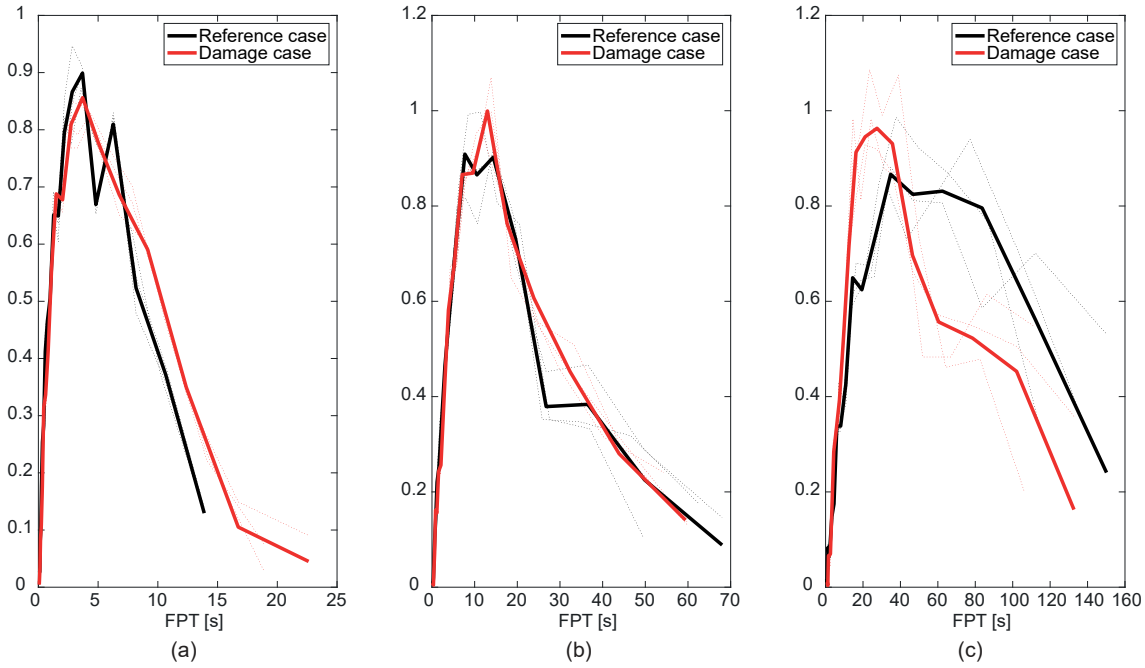

Figure 6: PDFs of FPT when the magnet is at point P_3: (a) at point II ($(X_0, X_f) = (0.96, 1.85)$), (b) at point III ($(X_0, X_f) = (0.96, 2.44)$) and (c) at point IV ($(X_0, X_f) = (0.96, 3.03)$)

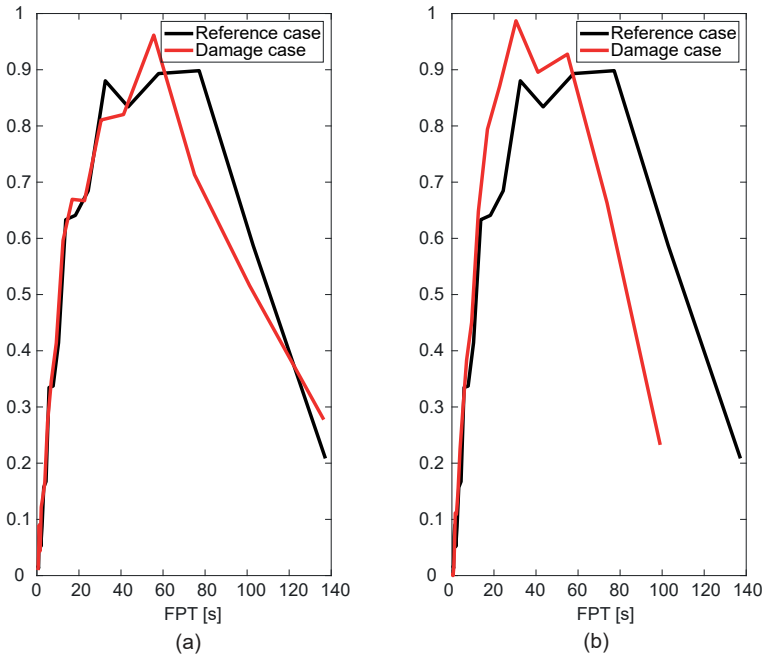

Figure 7: PDFs of FPT at point IV ($(X_0, X_f) = (0.96, 3.03)$) when the magnet is at points (a) P_1 and (b) P_2.

Table 2: P-values of the equivalence test for the absolute differences of statistical moments of FPT at points II, III, and IV and for $\alpha = 0.05$

	$\bar{m}$	$\bar{\sigma}$	$\bar{\gamma}_3$	$\bar{\gamma}_4$
II	$4.6494\,10^{-4}$(R)	0.0383(R)	0.3659(A)	0.3395(A)
III	0.8017(A)	0.9231(A)	0.5698(A)	0.4624(A)
IV	0.1135(A)	0.3831(A)	$2.2254\,10^{-4}$(R)	0.0058(R)

damaged case at point IV.

To determine whether two PDFs are equivalent or not, a more robust test can be done: the Kolmogorov-Smirnov (KS) test. In this case, the null hypothesis is that the two distributions are continuous and equal to each other. If the p-value obtained by the KS test is greater than $\alpha = 0.05$ then the null hypothesis is accepted (A) otherwise, the null hypothesis is rejected (R). The p-values of the KS test are provided in Table 3 for each damaged case P_i. It can be seen that for each damaged case, the KS test rejects the null hypothesis at location IV. Even if the PSDs do not show a major difference between the reference case and the damaged cases when the magnet is at points P_1 and P_2, the PDFs of FPT can capture slight structural behavioral modifications and therefore, they are a better indicator for early damage detection.

In Figure 7, the PDFs of FPT at point IV when the magnet is at points P_1 and P_2 are compared. A slight variation of the peak shape can be observed in Figure 7(a) while the peak location and the peak shape are distinctive in Figure 7(b) between the reference case and the damaged case. These observations support the results obtained by the KS test.

Table 3: P-values of the Kolmogorov-Smirnov test at points II, III, and IV when the magnet is at points P_1, P_2, P_3 and $\alpha = 0.05$

	P_1	P_2	P_3
II	0.5897(A)	$3.8643\,10^{-5}$(R)	$2.3482\,10^{-6}$(R)
III	0.0171(R)	$1.5822\,10^{-11}$(R)	0.1046(A)
IV	0.0423(R)	$7.4020\,10^{-23}$(R)	$2.4915\,10^{-26}$(R)

4 Conclusion

For the first time FPT maps have been applied to detect damage on a structure. The damage has been simulated by adding a small magnet to the test specimen. It has been placed at three different locations, P_i with $i = \{1, 2, 3\}$, to simulate various levels of damage. The velocity of the structure has been measured and its PSD has been computed for four different configurations: one reference case and the three damaged cases. No major difference on PSDs was observed for the first two locations P_i compared to the reference case.

By applying the Hilbert transform, the envelope of the measured velocity has been determined. Its FPT maps have been computed. In particular, the average FPT maps and the STD of FPT maps of the reference case and of the worst damaged case (when the magnet is at point P_3) have been compared. Two distinct regions have been defined: region A where the computed FPTs sharply increase for a small increment of X_f and region B where FPT values vary more smoothly. Visual insception reveals obvious differences in region A between the contours of the FTP maps obtained for the reference case and the damaged case. The FPT algorithm also returns PDFs of FPT for a chosen set $\{X_0, X_f\}$. Based on the occurrence map, it has been decided to compute four PDFs of FPT at locations I, II, III, and IV around $X_0 = 1$, where the number of occurrences is maximum. It has been observed that the PDFs of FPT possess various shapes among which a bimodal shape at the location I. As expected, no significant difference has been observed for PDFs of FPT at locations II and III because these PDFs are located inside region B. However, a large discrepancy has been shown by comparing the PDFs of FPT of the reference case and the damaged case at point IV. To support this observation, an equivalence test and a Kolmogorov-Smirnov test have been made. These tests have confirmed that the PDFs of FPT were different at point IV.

This analysis has been extended to the other two damaged cases when the magnet is at points P_1 and P_2. It follows that the PDFs of FPT at point IV are distinctive between the reference case and all damaged cases. This observation is remarkable in the sense that the damage would certainly not be detected based on traditional methods relying on changes in modal properties (in this case, the relative change of the natural frequency is only 0.15%). The more acute ability to detect changes is attributable to the fact that the proposed method provides much richer information, a complete map of statistics, or a set of FPT distributions, rather than a single scalar, obtained as the natural frequency of the (possibly damaged) structure. The method therefore becomes useful and very promising for early damage detection.

The next step will consist of studying whether the method can be extended to identify the location and magnitude of structural changes, based on the observation of the FPT maps only. Completion of these direct and indirect tasks will offer new perspectives on structural health monitoring based on FPT maps and the PDFs of FPT.

Acknowledgement

K. Theunissen has been supported by the Belgian Fund for Scientific Research.

References

[1] H. Vanvinckenroye and V. Denoël, "Average first-passage time of a quasi-hamiltonian mathieu oscillator with parametric and forcing excitations," *Journal of Sound and Vibration*, vol. 406, pp. 328–345, 10 2017.

[2] H. Vanvinckenroye and V. Denoël, "Second-order moment of the first passage time of a quasi-hamiltonian oscillator with stochastic parametric and forcing excitations," *Journal of Sound and Vibration*, vol. 427, pp. 178–187, 8 2018.

[3] H. Vanvinckenroye, T. Andrianne, and V. Denoël, "First passage time as an analysis tool in experimental wind engineering," *Journal of Wind Engineering and Industrial Aerodynamics*, vol. 177, pp. 366–375, 2018.

[4] E. Delhez, H. Vanvinckenroye, J.-C. Golinval, and V. Denoël, "Numerical and experimental study of first passage time of a steel strip subjected to forced and parametric excitations."

[5] E. Delhez, "Experimental and numerical study of first passage time. master thesis. university of liege. 2018 https://orbi.uliege.be/handle/2268/224212."

[6] K. Theunissen and V. Denoël, "An efficient algorithm for the numerical calculation of the first passage time maps of recorded signals," *Mechanical Systems and Signal Processing [Submitted]*.

[7] Supermagnete. Cube magnétique aimant cube 5 mm doré n50. [Online]. Available: https://www.supermagnete.be/fre/aimants-cube-neodyme/cube-magnetique-5mm{_}W-05-N50-G

[8] A. Preumont, *Vibrations aléatoires et analyse spectrale*, vol. 1. éd. Lausanne: Pr. Polytechniques et Univ. Romandes, 1990.